Molecular Structures of $M_2(CO)_9$ and $M_3(CO)_{12}$ (M = Fe, Ru, Os): New Theoretical Insights

Elke Hunstock,[†,‡] Carlo Mealli,[§] Maria José Calhorda,[‡,⊥] and Joachim Reinhold,*[,†]

Institut für Physikalische und Theoretische Chemie, Universität Leipzig, D-04103 Leipzig, Germany, Istituto per lo Studio della Stereochimica ed Energetica dei Composti di Coordinazione, CNR, I-50132 Firenze, Italy, Instituto de Tecnologia Química e Biológica, UNL, P-2781-901 Oeiras, Portugal, and Department of Chemistry and Biochemistry, Faculty of Science, University of Lisboa, P-1749-016 Lisboa, Portugal

Received May 14, 1999

A different number of bridging carbonyls is found in bi- or trinuclear clusters having the title formulas. Comparative calculations at the SCF, MP2, and DFT levels of theory show that only the latter is able to describe properly the energetics of various isomers of the whole triad. For the first-row transition metal, DFT gives excellent agreement with the experimental structures, whereas the MP2 approach fails completely. Conversely for the second- and third-row metals, the best agreement with the experiment is obtained by the MP2 optimizations. The quantitative computational results, associated with a qualitative MO analysis, allow one to conclude that the structural preferences are determined by a critical balance of metal−bridge bonding, metal−metal bonding, and intermetallic repulsion. Although the M−M bond order is expected to be 1 in all cases, the bridge-supported bond is experimentally and computationally shorter than the unsupported one. By contrast, the trend for the overlap population (OP) is reversed, with even negative values for the shorter bridge bonds. For the latter, only a weak attractive interaction stems from the almost pure t_{2g} orbitals, taken as metal lone pairs or eventually responsible for back-donation (formation of metal−bridge σ bonds). Thus, the negative OP values are consistent with a prevailing repulsion between the latter levels. In the iron systems, with more contracted metal orbitals, the direct metal−metal repulsion is relatively weak while the metal−bridge bonds are sufficiently strong. This is not equally true for the more diffuse ruthenium and osmium orbitals, so the alternative nonbridged structure is preferred.

Introduction

The 18-electron rule and its extensions to polynuclear systems apply also in the presence of carbonyl ligands although conceptual distinctions are needed. For terminal COs, the metal−carbon σ bond is due to the two-electron donation from the ligand, whereas two or four electrons used in back-donation and giving rise to multiple metal−carbon π bonding are counted as if they are *metal lone pairs*. In systems with bridging COs, the formal electron counting does not change (two electrons per CO) despite the presence of pairwise equivalent metal−carbon σ bonds. In agreement with the lower CO stretching frequencies, the electron density received by the bridging ligand in only one π^* level is greater than that received in two orthogonal π^* levels when CO is terminally bound. The border between the two situations is subtle as, for example, clusters with general formula $M_x(CO)_y$ and metals belonging to the same group feature different conformers with either all terminal or some bridging carbonyl ligands. For example, $Co_2(CO)_8$ may exist as a doubly bridged isomer or as one having only terminal carbonyls. Another classic case is that of $M_2(CO)_9$ dimers, where, for M = Fe, the triply bridged structure $(CO)_3Fe(\mu\text{-}CO)_3Fe(CO)_3$ (**1**) with D_{3h} symmetry is most stable.[1] On the contrary, osmium favors the C_{2v} singly bridged structure $(CO)_4Os(\mu\text{-}CO)Os(CO)_4$ (**2**) as indicated by IR spectroscopy[2] (see Chart 1, top).

Chart 1

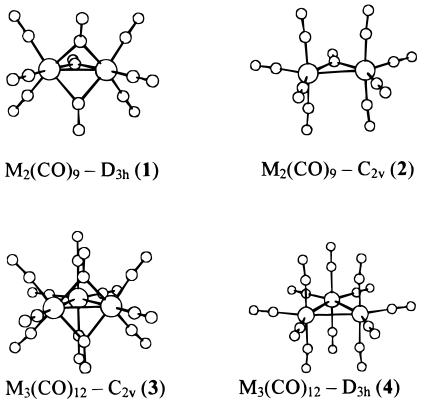

A corresponding situation arises for the $M_3(CO)_{12}$ trimers with either D_{3h} or C_{2v} symmetry (see Chart 1, bottom). For M = Fe, two of the metal centers are doubly bridged (**3**),[3] whereas for M = Ru and Os none of the M−M bonds are bridged (**4**).[4] Despite the many studies devoted to these species, their presentation in textbooks is not accompanied by some intuitive explanation for the different structural preferences.

[†] Universität Leipzig.
[‡] UNL.
[§] CNR.
[⊥] University of Lisboa.

(1) Cotton, F. A.; Troup, J. M. *J. Chem. Soc., Dalton Trans.* **1974**, 800.
(2) Moss, J. R.; Graham, W. A. G. *J. Chem. Soc., Chem. Commun.* **1970**, 835.
(3) (a) Cotton, F. A.; Troup, J. M. *J. Am. Chem. Soc.* **1974**, *96*, 4155. (b) Braga, D.; Grepioni, F.; Farrugia, L. J.; Johnson, B. F. G. *J. Chem. Soc., Dalton Trans.* **1994**, 2911.

10.1021/ic9905289 CCC: $18.00 © 1999 American Chemical Society
Published on Web 10/12/1999

Theoretical analyses at various levels of theory have been devoted to the electronic structure of $Fe_2(CO)_9$, especially to answer the question of whether a direct metal−metal bond exists. Such a bond is required to satisfy the 18-electron rule of each metal center as any experimentalist can predict. Theoreticians, however, are somewhat inclined to deny its existence because several arguments, e.g., the negative value of the calculated Fe−Fe overlap population (OP), better support an effective Fe−Fe repulsion.[5,6] However, a detailed analysis indicated that a small direct Fe−Fe attractive interaction is hidden under this relatively large repulsion.[6] Only a few attempts have been made to reproduce the experimental structure of the dimers by complete geometry optimization.[6b,7] An excellent agreement between theory and experiment has resulted from the DFT optimizations of Jacobsen and Ziegler[7a] and, more recently, by those of Schaefer et al.[7b]

Concerning the electronic and molecular structures of the trimeric systems, various calculations have been reported, for which semiempirical or X_α methods were employed.[8,9] A DFT investigation of the electronic structure of $Fe_3(CO)_{12}$ was carried out by Rosa and Baerends.[5c] $Fe_2(CO)_9$ and $Fe_3(CO)_{12}$ were considered to consist both of a doubly bridged $(CO)_3Fe(\mu\text{-}CO)_2Fe(CO)_3$ fragment and of a CO or an $Fe(CO)_4$ unit, respectively (see Chart 1). Recently, Schaefer et al. studied the electronic structure and determined the harmonic vibrational frequencies for both $Fe_2(CO)_9$ and $Fe_3(CO)_{12}$, using DFT techniques.[7b] The first SCF optimization for the osmium trimeric system was published by Morokuma et al.[10]

In this paper, we compare exhaustively the complete geometry optimizations of the structures **1**−**4** for the triad M = Fe, Ru, and Os at the SCF, MP2, and DFT levels of theory. The most plausible isomers are involved. Besides addressing the reliability of the different methods in dealing with different metals, the purpose of this work is to detect how the structural preferences for different isomers are originated. By referring the quantitative computational results to some basic concepts of qualitative MO theory, a rationale for the different strengths of bridged and nonbridged metal−metal bonds is presented.

Computational Details

Independent of the metal, D_{3h} symmetry was adopted for the triply bridged dimers and the nonbridged trimers. C_{2v} symmetry was assumed for the singly bridged dimers and for the doubly bridged trimers as well. Experimentally, it has been shown that the asymmetric bridges known for $Fe_3(CO)_{12}$ become progressively more symmetric as the temperature decreases, leading to an almost perfect C_{2v} symmetry.[3b]

The ab initio calculations at the SCF and MP2 levels were performed using the Turbomole program system.[11] For the metals, the inner shells (Fe, 1s−2p; Ru, 1s−3d; Os, 1s−4f) were replaced by the relativistic effective core potentials of Hay and Wadt, thus including the outermost core orbitals in the SCF procedure. These orbitals were fully contracted, while the (n - 1)d and np valence shells were described by a double-ζ basis completed by two np diffuse functions (n = principal quantum number).[12] For the ligand atoms C and O, standard basis sets (6-31G) were used. The structures resulting from the SCF and MP2 optimizations have been identified as minima on the potential surface by frequency analysis.

All density functional calculations were performed using the Amsterdam density functional program package.[13] The local spin density (LSD) exchange correlation potential[14a] was used with the local density approximation (LDA) of the correlation energy (Vosko−Wilk−Nusair).[14b] Becke's nonlocal corrections[15] to the exchange energy and Perdew's nonlocal corrections[16] to the correlation energy were used. Relativistic effects were considered for Ru and Os and were treated by a quasi-relativistic method where Darwin and mass−velocity terms are incorporated.[17] For the metals, the inner shells were frozen, and in the cases of Fe and Ru, the outermost core orbitals were added to the valence part and described by a double-ζ basis set. A triple-ζ basis set was used for the outermost (n − 1)d and ns shells of the three metals and of all ligand atoms. All metal bases were augmented by one diffuse np function.

The qualitative MO analysis was performed at the EHMO level[18] with the weight-modified Wolfsberg−Helmholz formula[19] as programmed in the package CACAO.[20] The cluster geometries were either the experimental ones or those optimized ab initio; however, adjustments were imposed for trimers to fix bridged and unbridged M−M distances all equal. This allows a comparative analysis of the OPs to be made without any bias. The newest version of CACAO[20b] has many utilities such as an interactive Molecular Editor (for example, experimental crystallographic coordinates are adapted to the nearest symmetry point group). Moreover, the possibility is given of generating molecular orbital overlap population (MOOP) diagrams which show how the overlap population of a given bond sums up MO by MO (see discussion below).

Results and Discussion

Molecular Structures. Selected structural parameters and energy values resulting from the optimizations are collected in Tables 1 and 2 for the dimers $M_2(CO)_9$ and the trimers M_3-

(4) (a) Churchill, M. R.; Hollander, F. J.; Hutchinson, J. P. *Inorg. Chem.* **1977**, *16*, 2655. (b) Churchill, M. R.; DeBoer, B. G. *Inorg. Chem.* **1977**, *16*, 878.

(5) (a) Summerville, R. H.; Hoffmann, R. *J. Am. Chem. Soc.* **1979**, *101*, 3821. (b) Bauschlicher, C. W. *J. Chem. Phys.* **1986**, *84*, 872. (c) Rosa, A.; Baerends, E. J. *New J. Chem.* **1991**, *15*, 815.

(6) (a) Mealli, C.; Proserpio, D. M. *J. Organomet. Chem.* **1990**, *386*, 203. (b) Reinhold, J.; Hunstock, E.; Mealli, C. *New J. Chem.* **1994**, *18*, 465.

(7) (a) Jacobsen, H.; Ziegler, T. *J. Am. Chem. Soc.* **1996**, *118*, 4631. (b) Jang, J. H.; Lee, J. G.; Lee, H.; Xie, Y.; Schaefer, H. F., III *J. Phys. Chem.* **1998**, *102*, 5298.

(8) (a) Korol'kov, D. V.; Miessner, H. *Z. Phys. Chem. (Leipzig)* **1973**, *253*, 25. (b) Schilling, B. E. R.; Hoffmann, R. *J. Am. Chem. Soc.* **1979**, *101*, 3456. (c) Tyler, D. R.; Levenson, R. A.; Gray, H. B. *J. Am. Chem. Soc.* **1978**, *100*, 7888. (d) Ajo, D.; Granozzi, G.; Tondello, E.; Fragala, I. *Inorg. Chim. Acta* **1979**, *37*, 191. (e) Delley, B.; Manning, M. C.; Ellis, D. E.; Berkowitz, J.; Trogler, W. C. *Inorg. Chem.* **1982**, *21*, 2247.

(9) (a) Evans, D. G. *J. Chem. Soc., Chem. Commun.* **1983**, 675. (b) Li, J.; Jug, K. *Inorg. Chim. Acta* **1992**, *196*, 89. (c) Braga, D.; Grepioni, F.; Tedesco, E.; Calhorda, M. J.; Lopes, P. E. M. *J. Chem. Soc., Dalton Trans.* **1995**, 3297.

(10) Riehl, J.-F.; Koga, N.; Morokuma, K. *Organometallics* **1993**, *12*, 4788.

(11) Ahlrichs, R.; Baer, M.; Baron, H. P.; Ehrig, M.; Haase, F.; Haeser, M.; Horn, H.; Koelmel, C.; Schaefer, A.; Schneider, U.; Weis, P.; Weiss, H. *TURBOMOLE*, Version 3.0 beta; University of Karlsruhe: Karlsruhe, Germany, 1992.

(12) (a) Hay, P. J.; Wadt, W. R. *J. Chem. Phys.* **1985**, *82*, 299. (b) Hay, P. J.; Wadt, W. R. *Technical Report*; Los Alamos National Laboratory: Los Alamos, NM, 1990.

(13) (a) *Amsterdam Density Functional (ADF) program*, release 2.2; Vrije Universiteit: Amsterdam, The Netherlands, 1995. (b) Baerends, E. J.; Elis, D. E.; Ros, P. *Chem. Phys.* **1973**, *2*, 42. (c) Boerrigter, P. M.; te Velde, G.; Baerends, E. J. *Int. J. Quantum Chem.* **1988**, *33*, 87. (d) te Velde, G.; Baerends, E. J. *J. Comput. Phys.* **1992**, *99*, 84.

(14) (a) Parr, R. G.; Yang, W. *Density Functional Theory of Atoms and Molecules*; Oxford University Press: New York, 1989. (b) Vosko, S. H.; Wilk, L.; Nusair, M. J. *Can. J. Phys.* **1980**, *58*, 1200.

(15) (a) Becke, A. D. *J. Chem. Phys.* **1986**, *84*, 4524. (b) Becke, A. D. *Phys. Rev.* **1988**, *A38*, 3098.

(16) (a) Perdew, J. P. *Phys. Rev.* **1986**, *B33*, 8822. (b) Perdew, J. P. *Phys. Rev.* **1986**, *B34*, 7406.

(17) (a) Ziegler, T.; Tschinke, V.; Baerends, E. J.; Snijders, J. G.; Ravenek, W. *J. Phys. Chem.* **1989**, *93*, 3050. (b) Snijders, J. G.; Baerends, E. J. *Mol. Phys.* **1978**, *36*, 1789. (c) Snijders, J. G.; Baerends, E. J.; Ros, P. *Mol. Phys.* **1979**, *38*, 1909.

(18) (a) Hoffmann, R.; Lipscomb, W. N. *J. Chem. Phys.* **1962**, *36*, 2872. (b) Hoffmann, R.; Lipscomb, W. N. *J. Chem. Phys.* **1962**, *37*, 3489.

(19) Ammeter, J. H.; Bürgi, H.-B.; Thibeault, J. C.; Hoffmann, R. *J. Am. Chem. Soc.* **1978**, *100*, 3686.

(20) (a) Mealli, C.; Proserpio, D. M. *J. Chem. Educ.* **1990**, *67*, 399. (b) Mealli, C.; Ienco, A.; Proserpio, D. M. *Book of Abstracts of the XXXIII ICCC*, Florence, 1998; Consiglio Nazionale delle Ricerche: p 510.

Table 1. Selected Structural Parameters (pm, deg) and Energy Values (kcal/mol) Resulting from the SCF, MP2, and DFT Optimizations of the Dimeric Systems $M_2(CO)_9$[a]

		$Fe_2(CO)_9$		$Ru_2(CO)_9$		$Os_2(CO)_9$	
		D_{3h}	C_{2v}	D_{3h}	C_{2v}	D_{3h}	C_{2v}
M−M	*exptl*	*252.3*					
	SCF	259.2	282.3	275.0	298.9	277.1	292.1
	MP2	246.1	277.9	283.5	289.4	285.7	290.7
	DFT[c]	*252.3*					
	DFT[d]	*251.9*					
	DFT[e]	*252.5*					
	DFT	249.3	271.2	278.8	298.9	285.3	303.5
$M-C_{br}$[b]	*exptl*	*201.6*					
	SCF	209.1	204.0	213.9	217.3	216.4	214.8
	MP2	190.4	202.9	218.4	218.8	220.6	220.1
	DFT[c]	*201.1*					
	DFT[d]	*200.7*					
	DFT[e]	*200.8*					
	DFT	199.8	199.5	215.8	215.5	222.4	221.4
$M-C_t/C_{out}$[b]	*exptl*	*183.8*					
	SCF	195.0	203.4	203.6	202.7	197.9	198.9
	MP2	169.1	170.6	194.9	194.2	194.0	196.0
	DFT[c]	*182.5*					
	DFT[d]	*181.9*					
	DFT[e]	*182.9*					
	DFT	181.1	180.9	196.5	195.5	200.8	200.6
$M-C_{in1/2}$[b]	*exptl*						
	SCF		198.6/197.4		199.4/204.6		195.2/199.2
	MP2		173.4/179.5		192.5/197.5		192.5/195.9
	DFT		177.6/182.1		192.5/197.3		195.9/202.2
$\angle M-C_{br}-M$	*exptl*	*77.6*					
	SCF	76.6	87.5	80.0	86.9	79.6	85.7
	MP2	80.5	86.4	80.9	82.8	80.7	82.6
	DFT	72.2	85.7	80.5	87.8	79.8	86.5
ΔE	SCF	0.0	−16.6	21.2	0.0	32.3	0.0
	MP2	0.0	−67.5	2.6	0.0	13.6	0.0
	DFT	0.0	3.3	−0.2	0.0	7.1	0.0

[a] Experimental values are averaged values from ref 1. [b] C_{br} and C_t indicate bridging and terminal C atoms, respectively. C_{in} and C_{out} denote terminal C atoms in and out of the $M-C_{br}$-M plane, respectively, in the C_{2v} structure (1 denotes the position trans and 2 denotes the position cis to the opposite M). [c] Reference 7a. [d] Reference 7b (BP86). [e] Reference 7b (B3LYP).

$(CO)_{12}$, respectively. It is evident that different quantum chemical procedures, namely, conventional ab initio methods vs density functional techniques, have peculiar advantages and disadvantages in reproducing the experimental geometries. The general trends can be illustrated as follows.

Compared to the experimental values, for the first-row metal, the M−C distances are too large at the SCF level and too short at the MP2 level. For the second- and third-row metals, however, the distances are only slightly too large at the SCF level but, in most cases, very satisfactory at the MP2 level. These results parallel those of Ehlers and Frenking for the M−C bonds in mononuclear hexacarbonyls.[21]

Our calculations show that the nonbridged M−M distances in the trimers behave quite similarly to those observed in the dimers. Thus, the SCF values come out too large, as also found by Morokuma et al. for the osmium trimer.[10] The MP2 distances are significantly too small for the iron system, but in excellent agreement with the experimental ones for the ruthenium and osmium systems (maximum deviation for the bond lengths, 1.3 pm).

The bond distances in the bridge regions exhibit another behavior. For the iron dimeric and trimeric systems, the $M-C_{br}$ and bridged M−M bonds are too long at the SCF level and too short at the MP2 level, as could have been expected. For the ruthenium and osmium systems, however, the $M-C_{br}$ bond distances increase at the MP2 level, indicating that, in these systems, the metal−bridge bonds are significantly weaker than the terminal metal−carbonyl bonds. Such an increase of the $M-C_{br}$ distances in doubly or triply bridged systems is associated with the increase of the corresponding M−M distances. In the singly bridged ruthenium and osmium dimers, however, the M−M distances slightly decrease with the consequence of a relatively large decrease of the $M-C_{br}-M$ bond angles. This is an indication that in the latter systems the bent M−M interaction is more direct and strongly correlated with the metal−CO bridge bonding.

Alternative methods to calculate complex molecular structures are based on the density functional theory. In recent investigations, the experimental structures of first-row transition-metal complexes have been successfully reproduced. For the triply bridged diiron nonacarbonyl, both Jacobsen and Ziegler[7a] and Schaefer et al.,[7b] using various DFT approaches, have found excellent agreement between theory and experiment. The deviations we have found, for this system, are slightly larger; nevertheless, the experimental geometry is fairly well reproduced (see Table 1). Analogously, for the iron C_{2v} trimer, the agreement between DFT optimizations and experiment is satisfactory (Table 2). It turns out that our results and those of Schaefer et al.[7b] are of comparable quality. We conclude that a similar reliability can be expected for the computations of both the C_{2v} dimer and the D_{3h} trimer of iron whose experimental structure is not available. On the other hand, for the ruthenium and osmium D_{3h} trimers (**4**), the agreement between experimental and calculated geometries is best by using the MP2 approach.

(21) (a) Ehlers, A. W.; Frenking G. *J. Chem. Soc., Chem. Commun*. **1993**, 1709. (b) Ehlers, A. W.; Frenking G. *J. Am. Chem. Soc*. **1994**, *116*, 1514. (c) Ehlers, A. W.; Frenking, G. *Organometallics* **1995**, *14*, 423.

Table 2. Selected Structural Parameters (pm, deg) and Energy Values (kcal/mol) Resulting from the SCF, MP2, and DFT Optimizations of the Trimeric Systems $M_3(CO)_{12}$[a]

		$Fe_3(CO)_{12}$		$Ru_3(CO)_{12}$		$Os_3(CO)_{12}$	
		C_{2v}[f]	D_{3h}	C_{2v}	D_{3h}	C_{2v}	D_{3h}
M−M(br)	*exptl*	*254.0*					
	SCF	276.5		284.5		283.6	
	MP2			285.1		286.3	
	DFT[c]	*257.2*					
	DFT[d]	*259.0*					
	DFT	256.5		286.1		296.8	
M−M(nbr)	*exptl*	267.5/268.2			*285.4*		*287.7*
	SCF[e]						*291.9*
	SCF	290.6	299.6	288.9	294.1	290.0	294.5
	MP2		240.1	279.3	283.5	283.4	287.1
	DFT[c]	*271.3*					
	DFT[d]	*273.6*					
	DFT	266.7	274.5	291.7	291.2	298.4	302.7
M−C_{br}[b]	*exptl*	*195−205*					
	SCF	209.8		214.7		216.2	
	MP2			217.1		219.1	
	DFT[c]	*199.6*					
	DFT[d]	*199.7*					
	DFT	199.5		215.6		223.7	
M−$C_{eq/in}$/C_{eq}[b]	*exptl*	*182*			*192.1*		*191.2*
	SCF[e]						*196.3*
	SCF	199.6/198.8	198.3	200.2/201.9	199.0	195.7/196.6	195.0
	MP2		164.5	192.7/191.8	192.3	192.8/192.4	192.5
	DFT[c]	*178.4/178.8*					
	DFT[d]	*179.9/189.0*					
	DFT	178.2/177.8	178.2	192.0/193.7	191.6	196.4/197.7	196.0
M−$C_{ax/out}$/C_{ax}[b]	*exptl*	*182*			*194.2*		*194.6*
	SCF[e]						*198.0*
	SCF	201.5/193.3	200.9	200.3/199.5	199.7	197.9/195.8	197.5
	MP2		170.2	194.9/193.6	194.7	195.9/193.1	195.8
	DFT[c]	*180.5/181.5*					
	DFT[d]	*181.4/182.5*					
	DFT	181.2/180.2	180.8	192.3/195.4	195.7	196.9/200.7	200.0
∠M−C_{br}−M	*exptl*	77.5/80.0					
	SCF	82.5		83.0		81.9	
	MP2			82.1		81.6	
	DFT	80.0		83.0		84.0	
ΔE	SCF	0.0	−18.1	9.9	0.0	26.7	0.0
	MP2	0.0		−1.9	0.0	9.0	0.0
	DFT	0.0	6.7	1.4	0.0	9.4	0.0

[a] Experimental values are averaged values from refs 3b and 4 for the Fe, Ru, and Os systems, respectively. [b] C_{br} indicates bridging C atoms. C_{eq} and C_{ax} indicate C atoms of the $M(CO)_4$ fragment in equatorial and axial positions, respectively. C_{in} and C_{out} indicate C atoms of the $M(CO)_3$ fragments in and out of the M_3 plane, respectively. [c] Reference 7b (BP86). [d] Reference 7b (B3LYP). [e] Reference 10. [f] No stationary point could be localized at the MP2 level.

Trends of the Calculated Energies. In general, the energy differences (ΔE) in Tables 1 and 2 are given relative to the experimentally known structural prototypes which are taken as the zero points. Since no structure of ruthenium dimers has ever been reported, the singly bridged structure (**2**) is chosen as the reference point in analogy to the known nature of the osmium analogue.

The DFT approach is able to reproduce consistently the experimental trends of the whole triad. Thus, the iron systems show an energetic preference for structures with more bridges (D_{3h} dimer and C_{2v} trimer), whereas, for osmium systems, just these structures are calculated to be the less stable ones. The ruthenium D_{3h} trimer is only slightly stabilized compared to the C_{2v} structure, whereas the calculations for the ruthenium dimer do not indicate a clear-cut energetic preference for any of the two structures considered.

At the SCF level, structures with more bridges appear to be generally less stable independently of the nature of the metal. At the MP2 level, the energetics of the iron systems are not too meaningful in view of the unrealistic geometries obtained. For the osmium systems, however, the MP2 energy differences are more trustworthy in view both of the quite good optimized geometry and of their agreement with the DFT results. For the ruthenium trimer, the bridged structure has the lower MP2 energy.

It can be concluded from both the DFT and MP2 calculations that the structures observed experimentally are only modestly preferred (ΔE < 10 kcal/mol) in comparison with the other possible isomers. Actually, for the iron systems, the SCF and MP2 methods fail, whereas, for the osmium systems, DFT and MP2 give the right energetic order. For the ruthenium systems, the energetic differences between the isomers are very close to zero at both the MP2 and DFT levels, and uncertainties remain.

Nature of Metal−Metal and Metal−Carbonyl Bonding. Qualitative MO analysis offers some reasonable explanations for the dichotomy of both the dimers (**1**, **2**) and the trimers (**3**, **4**). We start with simple considerations on electron counting. The system of two equations in (1) is an already proposed

$$\begin{aligned} 2m + n &= V - L \\ 2m + 2n &= T - 2L \end{aligned} \tag{1}$$

extension[22] of the effective atomic number (EAN) rule for

Chart 2

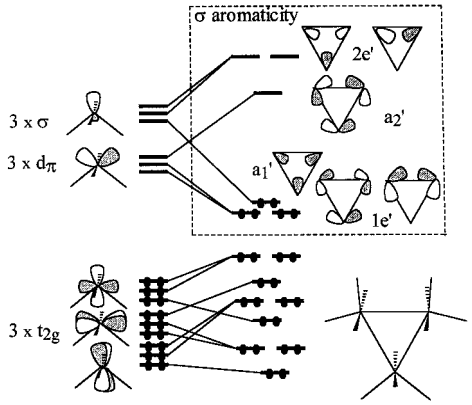

clusters which allows the prediction of not only the number m of M−M bonds but also the number n of lone pairs localized at the metal centers and eventually used in π-back-donation to terminal COs. In (1), V is the total number of available metal valence orbitals, T is the total metal valence electron count of the cluster, and L is the variable number of metal−carbon σ bonds. For the dimeric systems ($V = 2 \times 9 = 18$, $T = 34$), the solutions are $m = 1$, $n = 4$ and $m = 1$, $n = 6$ for the D_{3h} ($L = 12$) and C_{2v} ($L = 10$) clusters, respectively. For the trimeric systems ($V = 3 \times 9 = 27$, $T = 48$), $m = 3$, $n = 9$ and $m = 3$, $n = 7$ are obtained for the D_{3h} ($L = 12$) and C_{2v} ($L = 14$) clusters, respectively. These results are an important guideline in interpreting the architecture of the MOs in the different species, as besides the same number of filled MOs having M−M bonding character, the metal *lone pairs* (as well as the metal orbitals used in back-donation to the terminal carbonyls) are different for each geometry.

We concentrate the discussion on the trimeric systems, as the dimers have already been analyzed in detail using similar criteria.[9] In the D_{3h} isomers, each d^8-L_4M fragment with local C_{2v} symmetry has one σ and one d_π hybrid in the frontier region plus a set of three lower "t_{2g}" levels.[23] Chart 2 shows how the six frontier hybrids (with *radial* and *tangential* character with respect to the ring) give rise to three M−M bonding combinations ($m = 3$) and three antibonding ones. The latter situation is analogous to the σ aromaticity in cyclopropane,[24] a concept adapted also to other triangular metal clusters.[25]

Because the frontier hybrids have enough s and p character, their reciprocal overlap is good. This allows the formation of relatively strong M−M bonds despite significant electron repulsions between the nine lone pairs ($n = 9$). On the other hand, the latter effect is mitigated because a good part of the t_{2g} electron density is back-donated into the π^* orbitals of the terminal COs.

In the C_{2v} isomer, only the unique d^8-L_4M fragment has the same frontier σ and d_π hybrids used in the delocalized bonding of the D_{3h} species. The other two metal centers, in local square pyramidal geometry, overlap well with their *in-phase* and *out-of-phase* combinations of axial hybrids as shown in Charts 3 and 4.

The latter $2b_2$ and $2a_1$ MOs, which account for the two nonbridged M−M bonds, correspond to the second and third

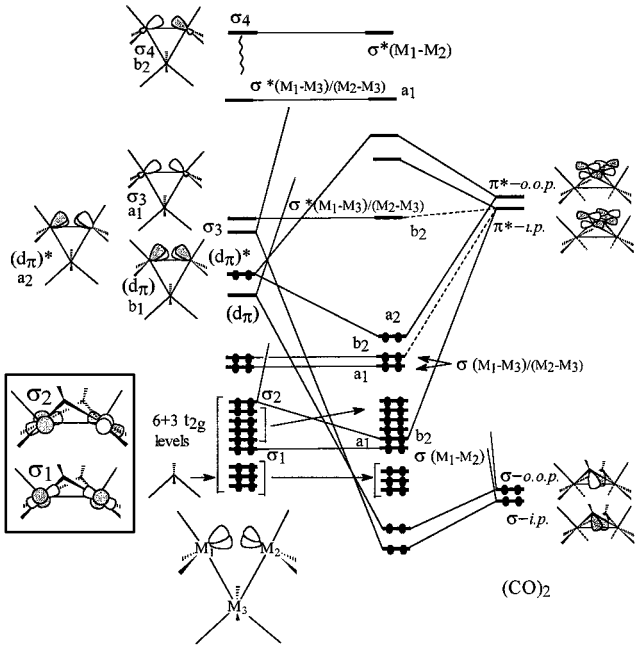

Figure 1. A general diagram for the interaction between two bridging carbonyls and the remaining part of the C_{2v} cluster $M_3(CO)_{12}$.

Chart 3

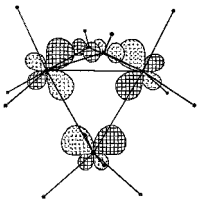

$2b_2$

Chart 4

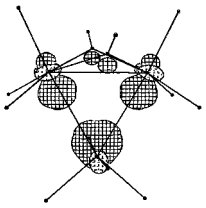

$2a_1$

HOMOs of the system, respectively (see Figure 1). At higher energies, the corresponding σ^* MOs, $3b_2$ and $3a_1$, are similar to $2b_2$ and $2a_1$ with the inverted phase at the unique metal atom. In particular, $3b_2$ (LUMO) lies much lower than $3a_1$ because, as $2b_2$, it has the stabilizing interaction with the bridging CO π^* orbitals. Analogously, it maintains the σ^* character for the bridged bond. Indeed, the nature of the latter linkage is rather complex. While the main bonding contribution arises from one or more MOs quite deep in energy, contrasting effects are due to the HOMO (a_2 shown in Chart 5), the second HOMO (Chart 3), and another lower b_2 level (Chart 6). As pointed out in refs 5a, 6, and 9c, all of the latter orbitals are bonding for the overall M−(CO)−M linkage but antibonding for the M−M bridge bond.

The detailed analysis of the interactions between the two bridging carbonyls (right side of Figure 1) and the rest of the molecule (left side) has already been presented in ref 9c. Here, the diagram is proposed again to highlight in particular the electronic nature of the M−M bridge bond.

(22) (a) Mealli, C.; Proserpio, D. M. *J. Am. Chem. Soc.* **1990**, *112*, 5484. (b) Mealli, C.; Lopez, J. A.; Yan, S.; Calhorda, M. J. *Inorg. Chim. Acta* **1993**, *213*, 199.
(23) Albright, A.; Burdett, J. K.; Whangbo, M. H. *Orbital Interactions in Chemistry;* Wiley: New York, 1985.
(24) Dewar, M. J. S. *J. Am. Chem. Soc.* **1984**, *106*, 669.
(25) Mealli, C. *J. Am. Chem. Soc.* **1985**, *107*, 2245.

Chart 5

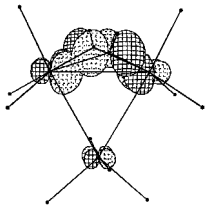

a_2

Chart 6

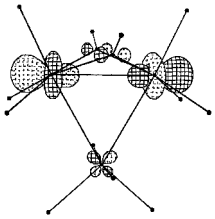

$1b_2$

Before interaction with the CO bridges, the metal atoms M_1 and M_2 have locally the shape of the L_4M fragments with C_{2v} symmetry, their common axial position being formed by the third metal fragment itself. The localized hybrids at the two metal centers correspond to four high levels of the fragment, i.e., the in-phase and out-of-phase combinations of the σ and d_π hybrids. Moreover, we must consider two sets of filled t_{2g} orbitals at the equivalent metals plus those of the unique L_4M fragment.

The bridging carbonyls direct their low-lying σ-donor orbitals toward the in-phase combinations of the σ and d_π hybrids at the metals, thus forming two M−(CO)−M bridge bonds. A third bond results from back-donation from the formally filled d_{π^*} trimetal fragment orbital into the $(\mu\text{-CO})_2$ π^* out-of-phase combination. The other expected back-donation into the π^* in-phase combination of $(\mu\text{-CO})_2$ is the least efficient as it involves the low-lying σ_2 out-of-phase combination of t_{2g} orbitals (see $1b_2$ in Chart 6). Additional back-donation of b_2 symmetry is observed also in the MO $2b_2$ taken as a major M−M nonbridged bonding MO (see Chart 3). The situation is analogous to that of the dimer $Fe_2(CO)_9$[6a] where one of the six metal−carbonyl bridge bonds was attributed to the back-donation from a low-lying unhybridized out-of-phase combination of z^2 orbitals (t_{2g}) into the proper $(\mu\text{-CO})_3$ π^* in-phase combination (a_2''). The weakness, but not the absence, of the latter interaction was also envisaged by specific ab initio calculations.[6b] In any case, the back-donation of this type is conceptually important to support eventually the existence of the M−M bridge bond in both $Fe_2(CO)_9$ and $Fe_3(CO)_{12}$ species. As indicated in Figure 1, the filled MOs derived from the FMOs σ_1 and σ_2 carry implicit σ and σ^* character for the pair of atoms M_1 and M_2. Their repulsion diminishes the more electron density is driven toward the bridging COs through the back-donation from σ^*. By assuming that the latter effect could be maximized, the M−M bonding of the σ_1 level would not be diminished by the antibonding counterpart σ_2 (rather, the high-energy $\sigma^*(M_1-M_2)$ level, derived from σ_4, becomes the specific antibonding partner of σ_1). Notice that such a formal description of the M−M single bond involves the participation of two metal *lone pairs* (originally nine) in full agreement with that predicted by (1). Essentially, one combination of lone pairs (σ_1) assumes a M−M bonding function while a second one (σ_2) is involved in M−(CO)−M bridge bonding. Thus, the more effective the back-donation of b_2 symmetry, the stronger the direct M−M bonding interaction between the bridged centers.

Table 3. Overlap Populations of the Bridged and Nonbridged M−M Bonds Resulting from the DFT Optimizations of the Dimeric and Trimeric Systems

	three bridges, $M_2(CO)_9$, D_{3h} (**1**)	two bridges, $M_3(CO)_{12}$, C_{2v} (**3**)	one bridge, $M_2(CO)_9$, C_{2v} (**2**)	no bridges, $M_3(CO)_{12}$, D_{3h} (**4**)
Fe−Fe(br)	−0.132	0.006	−0.043	
Ru−Ru(br)	−0.171	−0.113	−0.007	
Os−Os(br)	−0.124	−0.056	−0.048	
Fe−Fe(nbr)		0.070		0.081
Ru−Ru(nbr)		0.144		0.000
Os−Os(nbr)		0.002		0.030

Chart 7

Analysis of the Overlap Populations. The above qualitative arguments may be quantified by the Mulliken OP values for the M−M bonds. Table 3 reports the M−M OPs for the different $M_2(CO)_9$ and $M_3(CO)_{12}$ isomers as obtained from the DFT optimizations which produced the most reliable molecular geometries. Recall that the OPs between two given atoms are calculated by summing up the contributions of each occupied MO. These values are positive or negative depending on whether the interaction in the corresponding MO is bonding or antibonding.

As a general result for the present dimers and trimers, the OP values are positive for the nonbridged M−M bonds and negative for the bridged ones. The negative Fe−Fe overlap population obtained for $Fe_2(CO)_9$ (**1**), which is reproduced also by the present DFT calculations, has been considered by some authors as the proof that no Fe−Fe bond can be invoked. Elsewhere,[6] we have pointed out the possible origin of such a bond. Also it was emphasized that the degenerate HOMOs, shown in Chart 7, are strongly metal−bridge bonding as well as M−M antibonding. Thus, electrons in the latter are largely responsible for the negative M−M OP values in the D_{3h} dimers. In the C_{2v} dimers, only one orbital of this type exists and significantly less negative values follow.

In the C_{2v} trimers, two nondegenerate metal−bridge bonding and M−M antibonding orbitals exist, one of them being less effectively overlapping and, therefore, giving rise to less negative OPs (compared to the D_{3h} dimer) or, in the iron case, a small positive value for the unique bridge bond. These values are curious especially if related to the significantly more positive values of the nonbridged M−M linkages. The latter are found experimentally longer although the bond order is predictably equal to 1 in all cases. Also the EHMO calculations for the iron C_{2v} trimer show a consistent trend as the OP value of the bridge bond is slightly positive (similarly to the DFT result) but definitely smaller than that of the nonbridged bonds.

MOOP diagrams[20b] permit one to evaluate how the OP of any given bond sums up MO by MO. The idea is similar to that of COOP (crystal orbital overlap population) adopted in solid-state calculations.[26] It may be evaluated how the progressive population of levels affects a given bond.

The two MOOP diagrams of Figure 2 compare the bridged (left side) vs the nonbridged (right side) Fe−Fe bond in the

(26) (a) Hoffmann, R. *Solids and Surfaces—A Chemist's view of Bonding in Extended Structures*; VCH: Weinheim, 1988. (b) Hoffmann, R. *Angew. Chem., Int. Ed. Engl.* **1987**, *26*, 846−878.

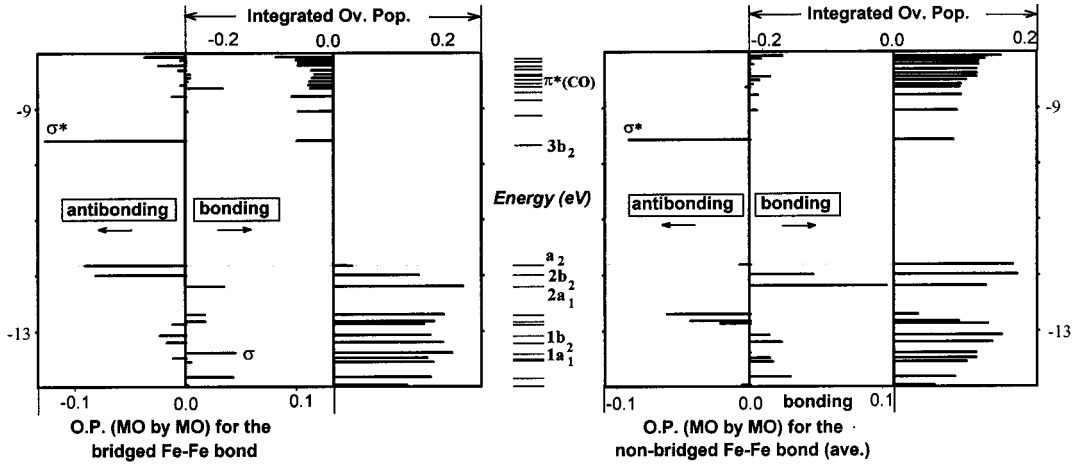

Figure 2. MOOP diagrams comparing the building up of the overlap population for the two types of Fe−Fe bonds in the C_{2v} structure of $Fe_3(CO)_{12}$. The energy range is restricted across the HOMO region (dashed line).

C_{2v} model (**3**) of $Fe_3(CO)_{12}$. The features are best understood having handy the MO scheme of Figure 1.

The bonding or antibonding character of any MO in the energy range −14 to −8 eV is easily envisaged for the two linkages. Moreover, the integrated OP values are reported (see legends at the top). This allows one to monitor how the bond builds up on populating effectively the levels up to the HOMO (the dotted line corresponds to the energy of the HOMO or Fermi level) and potentially over it. Thus, the left diagram, for the bridged bond, shows clearly the σ^* character of the two highest occupied a_2 and b_2 MOs (see Charts 3 and 5). The integration shows that, on populating the latter, all the bonding produced in the lower levels is wiped out. In particular, the σ MO (derived from the interaction between t_{2g} orbitals) lies low while small contributions given by other levels are equally low lying. Although not shown because out of the energy range, the $\sigma^*(M_1-M_2)$ level (derived from σ_4 in Figure 1) is more than 1 order of magnitude larger than any other antibonding MO.

Importantly, the LUMO $3b_2$, which has been indicated as σ^* for the unsupported Fe−Fe linkages, appears almost equally antibonding also for the unique linkage (compare the two diagrams). The complex nature of the MO $3b_2$ has been amply described in detail in the previous section; thus, the feature in the MOOP diagram is not very surprising. On the other hand, the diagram on the right side confirms that the nonbridged bonds are maximized with the population of the third and second HOMOs, and that the HOMO itself (Chart 5) has no effect. Bond weakening occurs with the LUMO, while several π^* CO levels appearing at the top have almost no effect.

Conclusive Remarks

Some studies have been devoted to interpreting the causes for the different structural isomers of polynuclear transition-metal carbonyls.[9,27,28] In early papers, attention was focused on the different polyhedral arrangements of the carbonyl groups which can accommodate M_n units of different size.[27] Moreover, the dynamics of the unit inside the polyhedron has been addressed. From force field molecular mechanics simulations[28] it has been concluded that steric effects alone cannot describe the differences between the iron and the ruthenium and osmium trinuclear systems. In summary, the importance of the electronic effects in fixing the structural trends seems to prevail.[9] Already, Evans[9a] and Li and Jug[9b] concluded from qualitative arguments that the contracted iron 3d orbitals are not so effective in both direct M−M bonding and π back-bonding to terminal carbonyls; thus, a number of metal−carbon bridge bonds are preferred. Conversely, the more diffuse and polarizable d orbitals of the ruthenium or osmium atoms should increase both the strength of M−M bonding and the back-donation to terminal COs. Detailed theoretical analyses of the problem based on EHMO calculations have been reported for the present and some related carbonyl clusters.[9c,29] It is discussed that in the bridged $M_3(CO)_{12}$ clusters the first two HOMOs are responsible for M−(CO)−M bridge bonding which have, at the same time, a clear-cut M−M antibonding nature. If the metal orbitals are diffuse (second and third transition rows), the M−M repulsion overwhelms the overall M−(μ-CO)−M attraction and the nonbridged structure is preferred.

A basic point of the present analysis concerns the relation between bond lengths and bond strengths, usually assumed directly proportional in chemistry. We have pointed out the incongruence for the C_{2v} trimers $M_3(CO)_{12}$. Namely, the bridged bond, which is shorter that the nonbridged ones, is also evidently weaker in terms of the OP values. The quantitative data can be compared by looking at Tables 1 and 2.

In switching from a noncorrelated (SCF) to a correlated (MP2) method, for the ruthenium and osmium systems, the distances between the metals and the bridging carbon atoms are elongated. Conversely, the terminal M−C bonds are strengthened most likely due to the diffuse nature of the metal orbitals and their high polarizability. For the iron systems, however, both the $M-C_t$ and the $M-C_{br}$ distances decrease on switching from SCF to a correlated level (either MP2 or DFT). The result is in line with the contracted and less polarizable nature of the iron orbitals and points to relatively strong Fe−(μ-CO)−Fe bridge bonding.

Concerning the effective direct repulsion between two bridged metal centers, the $M-C_{br}-M$ bond angles resulting from the DFT optimizations are a useful term of comparison. In the ruthenium and osmium D_{3h} dimers, the angle is significantly larger than in the corresponding iron system. As a consequence,

(27) Johnson, B. F. G. *J. Chem. Soc., Chem. Commun.* **1976**, 211.
(28) (a) Lauher, J. W. *J. Am. Chem. Soc.* **1986**, *108*, 1521. (b) Sironi, A. *Inorg. Chem.* **1996**, *35*, 1725.
(29) (a) Braga, D.; Grepioni, F.; Calhorda, M. J.; Veiros, L. F. *Organometallics* **1995**, *14*, 1992. (b) Braga, D.; Grepioni, F.; Wadepohl, H.; Gebert, S.; Calhorda, M. J.; Veiros, L. F. *Organometallics* **1995**, *14*, 5350. (c) Grepioni, F.; Braga, D.; Byrne, J.; Calhorda, M. J. *J. Chem. Soc., Dalton Trans.* **1995**, 3287.

the M−M distance is even larger than that expected because of the longer M−C_{br} bonds. This indicates a stronger repulsion between second- and third-row metals as a consequence of the more diffuse character of the ruthenium and osmium d orbitals, which increases the antibonding character of the relevant orbitals.

Analogously, the M−C_{br}−M bond angles increase for the C_{2v} trimers of the second- and third-row metals, reaching values as high as ca. 84°. This flexibility, which ensues from the reduced number of bridges, permits the further elongation of the M−M distance, and hence a reduced M−M repulsion (for example, compare in Table 3 the Ru−Ru OP values of −0.171 and −0.112 for the D_{3h} dimer and the C_{2v} trimer, respectively).

Finally, the opening of the M−C_{br}−M bond angles in C_{2v} dimers does not seem to follow any particular order. Since the bridging unit is rather flexible, the minimization of the electronic repulsion through the M−M elongation is facilitated.

It can be concluded that the reason for the different structures of the polynuclear transition-metal carbonyls depends strongly on the extent of the metal−bridge interactions. In the iron systems, with contracted metal orbitals, the metal−bridge bonds are relatively strong and the metal−metal repulsion is relatively weak, whereas in the ruthenium and osmium systems, with diffuse metal orbitals, the situation is just the opposite. Consequently, iron carbonyls tend to form bridge bonds, whereas ruthenium and osmium systems try to avoid such bonds.

Acknowledgment. J.R. and E.H. thank the Deutsche Forschungsgemeinschaft and the Fonds der Chemischen Industrie and M.J.C. and E.H. thank the TMR "Metal Clusters in Catalysis and Organic Synthesis" for financial support.

IC9905289